Fluorine Anion-Doped Ultra-Thin InGaO Transistors Overcoming Mobility-Stability Trade-off

J. Zhang[1,2], Z. Zhang[1], H. Dou[3], Z. Lin[1], K. Xu[3], W. Yang[2], X. Zhang[3], H. Wang[3] and P. D. Ye[1,*]
[1]School of Electrical and Computer Engineering, Purdue University, West Lafayette, IN, USA, *Email: yep@purdue.edu
[2] Department of Microelectronics and Integrated Circuit, Xiamen University, Xiamen, China
[3]School of Materials Engineering, Purdue University, West Lafayette, IN, USA

Abstract**—** In this work, we report on the first demonstration of back-end-of-line (BEOL)-compatible ultra-thin (~3 nm) fluorine-doped InGaO thin film transistors (TFTs) with scaled channel length (L_{ch}) down to 60 nm, achieving E-mode operation with highest I_{on}/I_{off} of ~10^{11}, high I_{on} of 418 μA/μm, low subthreshold swing (SS) of 85 mV/dec and remarkably high degree of thermal and bias stability among recently reported oxide TFTs. It is found that F-doping delivers better mobility-stability trade-off compared to that of Ga-doping, providing higher mobility and significantly enhanced stability performance simultaneously, which is attributed to the fact that F-doping could effectively reduce oxygen vacancy (V_O) donor traps and introduce metal-metal (M-M) bond acceptor traps without altering the conduction band edge (E_C). This study for the first time shows that anion doping has more advantages than commonly studied cation doping, thus points to a new research direction of studying the critical role of anion dopants in mobility-stability trade-off in oxide semiconductor TFTs.

I. Introduction

There is an increasing research interest in In_2O_3-based TFTs with scaled device dimension as BEOL transistors towards monolithic 3D integration [1-12]. These BEOL-compatible In_2O_3-based TFTs with sub-100 nm channel length (L_{ch}) exhibit high on-current (I_{on}) with channels formed by atomic layer deposited (ALD) or sputtering techniques [4-22]. Such high I_{on} could be attributed to the effective overlap of In 5s orbitals and rich oxygen vacancy (V_O) functioning donor traps naturally. These V_O defects, arising from the weak In-O bonds, benefit to the high I_{on} and mobility but also give rise to high off-current (I_{off}) and undesirable negative threshold voltage (V_T). Furthermore, V_O defects could be ionized under thermal or bias stress, leading to severe stability issues [20,23]. Doping In_2O_3 with other metal cations as strong oxygen binders has been shown experimentally to tune V_T positively, reduce I_{off} and improve stability effectively [3-22]. Short-channel IWO [7,8], ITO [9-12], IZO [13,14] and IGZO [15-19] TFTs with positive V_T (E-mode) has been reported. Compared to other cation dopants, Ga with small radius, high ionic potential and strong Ga-O bond, could be as an effective carrier suppressor to In_2O_3. Surprisingly, short-channel E-mode InGaO TFTs has not been demonstrated yet [22,23]. On the other hand, although cation doping could achieve E-mode and improve stability by suppressing V_O, the electron transport is also significantly hindered due to the altered E_C, leading to severe mobility-stability trade-off [2]. In this regard, anion doping, such as F-doping, could be more effective to passivate V_O defects, form strong In-F bonds and maintain preferred transport properties of In_2O_3. However, anion doping is generally neglected compared to cation doping with only few reports demonstrated in oxide semiconductor TFTs research [24,25].

In this work, we demonstrate for the first time E-mode F-doped InGaO TFTs with channel thickness (T_{ch}) of 3 nm and L_{ch} down to 60 nm, achieving highest I_{on}/I_{off} of ~10^{11} (I_{off} at V_{GS} of 0 V), high I_{on} of 418 μA/μm and low SS of 85 mV/dec among other reported oxide TFTs. Furthermore, F-doped In-rich InGaO TFTs exhibit higher field-effect-mobility (μ_{FE}) and significantly improved stability performance at the same time including alleviated self-heating-effect (SHE), enhanced temperature stability (3.1 mV/°C), and remarkably high positive gate bias thermal stability (PBTS) at 80 °C compared to that with higher Ga-doping (also E-mode), thus providing a new research direction of overcoming mobility-stability trade-off by the development of anion-doping techniques. The main achievements of this work are illustrated in Fig.4.

II. Experiments

The device fabrication flow, experimental procedure of Ga- and F-doping, and 3D device schematic of InGaO TFTs are presented in Fig.1. The InGaO TFTs are back-gate structure with 40 nm Ni, 6 nm HfO_2 and 3 nm InGaO as electrodes, dielectric, and semiconductor channel, respectively. The fabrication started with bottom gate formation using 40 nm Ni by photolithography and e-beam evaporation. Next, 6 nm HfO_2 dielectric was deposited by ALD at 200 °C, followed by the deposition of 3 nm InGaO by ALD at 225 °C. The Ga-doping level of InGaO channel was controlled by ALD cycle ratio. Two cycle ratios of 10:1 and 5:1 between In_2O_3 and Ga_2O_3 were applied to investigate the effects of Ga-doping, denoted as $In_{10}GaO$ and In_5GaO hereafter. Then, channel isolations were formed by ICP etching. Finally, 40 nm Ni was deposited as source/drain contacts by e-beam evaporation, defined by electron beam lithography. The fabricated TFTs have a L_{ch} ranging from 2 μm to 60 nm. For the F-doping, CF_4/N_2O plasma was applied on $In_{10}GaO$ samples at 200 °C for 1 min, denoted as $In_{10}GaO$:F hereafter. The details on fluorination process could be found in our previous work [24]. Figs.2 show the STEM image of $In_{10}GaO$ TFTs with L_{ch} of 60 nm, where both In and Ga can be clearly detected in the channel. The XPS spectrum were performed for film composition analysis in Figs.3. In_5GaO films show higher Ga concentration of 7.8 at% compared to that of 3.5 at% for $In_{10}GaO$ films, while ~6.7 at% F was doped into $In_{10}GaO$ film after F plasma treatment. Electrical characterization of TFTs were carried out in N_2 ambient with the Keysight B1500 system. The V_T of TFTs is extracted by linear extrapolation of transfer curves at V_{DS} of 0.05 V and multiple TFTs were measured for statistics with typical characteristics shown.

979-8-3503-2767-0/23/$31.00

III. Results and Discussion

Fig.5(a) shows bi-directional transfer curves of TFTs with L_{ch} of 1 μm, 400 nm and 60 nm, where similar switching behaviors can be observed for TFTs of same channel material and different L_{ch}. Such excellent short-channel immunity could be due to excellent electrostatic control using ultrathin channel and dielectric. All TFTs show negligible hysteresis and steep SS below 100 mV/dec, suggesting excellent dielectric/channel interface. Both Ga- and F-doping is found to tune V_T of TFTs positively as shown in Fig.5(b), where $In_{10}GaO$ TFTs show D-mode operation in contrast to that both $In_{10}GaO$:F and In_5GaO TFTs feature E-mode operation with more positive V_T in F-doped TFTs. Fig.5(c) exhibits transconductance (g_m) as a function of L_{ch}, which agrees well with $1/L_{ch}$ trend, suggesting low contact resistance (R_C) of TFTs. The μ_{FE} is extracted from long-channel TFTs with L_{ch} of 2 μm in Fig.5(d) without considering R_C. The μ_{FE} is reduced from 29.2 $cm^2/V\cdot s$ ($In_{10}GaO$) to 20.2 $cm^2/V\cdot s$ (F-doping) and 12.6 $cm^2/V\cdot s$ (Ga-doping). The reduced μ_{FE} arising from reduced electron concentration (positively shifted V_T) could be explained by the percolation mechanism in ultrathin amorphous channel. F-doping is found to deliver better V_T-μ_{FE} trade-off, providing higher μ_{FE} at more positive V_T.

Figs.6 show the transfer curves of TFTs with L_{ch} of 60 nm under various V_{DS}. Both $In_{10}GaO$ and In_5GaO TFTs exhibit negative V_T shift (ΔV_T) with increased V_{DS} until TFTs losing switching properties and becoming malfunctional. Such negative ΔV_T could be explained by the formation of donor traps (possibly ionized V_O) due to SHE with increased V_{DS} and I_{DS}. The In_5GaO TFTs are also found to sustain higher V_{DS} than that of $In_{10}GaO$ TFTs (Fig.7(a)), suggesting that Ga-doping could reduce donor traps. On the other hand, it is interesting to note that $In_{10}GaO$:F TFTs exhibit positive ΔV_T with increased V_{DS} and show much wider V_{DS} operation range. It is believed that acceptor traps may be introduced by F-doping in addition to reducing donor traps. These acceptor traps could function as trap sites under high V_{DS}, resulting in positive ΔV_T and significantly alleviating the loss of channel control due to SHE. A high g_m of 264 μS/μm could also be obtained in $In_{10}GaO$:F TFTs with L_{ch} of 60 nm under V_{DS} of 2 V (Fig.7(b)), slightly lower than that of $In_{10}GaO$ TFTs (325 μS/μm at V_{DS} of 0.8 V), which is also among the best values for oxide TFTs. Figs.8 show output characteristics of TFTs with L_{ch} of 60 nm, where high I_{on} of 1120, 386 and 418 μA/μm could be achieved in $In_{10}GaO$, In_5GaO, and $In_{10}GaO$:F TFTs, respectively. It should be emphasized that $In_{10}GaO$:F TFTs exhibit better current saturation with larger achievable V_{DS}. Note that a better current saturation is critical for RF transistors to achieve higher output resistance and higher f_{max} [26]. Fig.9 benchmarks I_{on}/I_{off} (I_{off} at V_{GS} of 0 V) versus achievable I_{on} of recently reported oxide TFTs with sub-100 nm L_{ch}. This work presents the first demonstration of scaled InGaO TFTs, achieving E-mode operation with highest I_{on}/I_{off} of ~10^{11} and good I_{on}.

Figs.10 present transfer curves of TFTs with L_{ch} of 100 nm under thermal stress up to 80 °C. It is found that both Ga- and F-doping could enhance thermal stability of TFTs and F-doped TFTs show remarkably thermal stability up to 80 °C. Fig.11(a) shows extracted V_T as a function of stress temperature, where temperature sensitivity reduces from 29 mV/°C ($In_{10}GaO$) to 6.4 mV/°C (In_5GaO) and 3.1 mV/°C ($In_{10}GaO$:F). The improved thermal stability could also be related with altered trap distribution, agreeing with the alleviated SHE. Thermal activated I_{DS} under different V_{GS} are shown in Fig.11(b), from which the activation energy (E_a) is extracted in Fig.12(a). Both Ga- and F-doping could increase E_a, reducing excessive electrons and realizing E-mode operation. $In_{10}GaO$:F TFTs achieve similar low E_a to that of $In_{10}GaO$ under high V_{GS}, whereas In_5GaO TFTs still exhibit a relatively high E_a. This could explain a lower μ_{FE} in In_5GaO TFTs due to the altered E_C by Ga-doping. O 1s spectrum (Fig.12(b)) suggests the reduced V_O by Ga- or F-doping. V_O functions as donor traps, being consistent with our previous explanation.

Comprehensive bias stability tests were performed in Figs.13-16. The $In_{10}GaO$ TFTs show negative ΔV_T in both NBS and PBS test at 25 °C. The anomalously negative ΔV_T under PBS test can be explained by the rich donor traps such as V_O. Due to the reduced donor traps, both In_5GaO and $In_{10}GaO$:F TFTs show normal positive ΔV_T in PBS test. Note that $In_{10}GaO$:F show more positive ΔV_T in PBS test and insignificant negative ΔV_T in NBS test than that of In_5GaO. It indicates the introduction of acceptor traps by F doping. This may also explain the results of PBTS test at 80 °C. Both $In_{10}GaO$ and In_5GaO TFTs exhibit large negative ΔV_T whereas F-doped TFTs show negligible ΔV_T of 27 mV under 3.4 MV/cm electrical stress and stress time of 1 ks at 80 °C. High temperature and bias could accelerate the formation of donor traps (ionized V_O), which is now effectively suppressed due to F-doping induced acceptor traps. Fig.17 benchmarks I_{on}/I_{off} versus stability $|1/\Delta V_T|$ of various oxide TFTs, where our F-doped InGaO TFTs stand out with highest I_{on}/I_{off} and remarkably high stability. This achievement is ascribed to the fact that F-doping changes trap distribution without altering E_C, providing a better mobility-stability trade-off (Fig.18).

IV. Conclusion

In conclusion, we report the first demonstration of E-mode F-doped InGaO TFTs with T_{ch} of 3 nm and L_{ch} down to 60 nm, achieving highest I_{on}/I_{off} of ~10^{11}, high I_{on} of 418 μA/μm and remarkably high degree of thermal and bias stability. This study discloses the critical role of dopants in mobility-stability trade-off and points to the importance of anion-doping technique in oxide semiconductor TFTs research. The work is supported by AFOSR, SRC nCore IMPACT Center and DARPA/SRC JUMP ASCENT Center.

References

[1] T. Kim *et al.*, Adv. Mater., 2023. [2] Y. Shiah, *et al.*, Nat. Electron., 2021. [3] M. Si et al., Nano. Lett., 2021. [4] M. Si et al., Nat. Electron.,2022. [5] P.Y. Liao *et al.*, IEDM, 2022. [6] A. Charnas *et al.*, APL, 2021. [7] W. Chakraborty *et al.*, TED, 2020. [8] Y. Hu et al., IEDM, 2022. [9] S. Li et al., IEDM, 2020. [10] Z. Zhang *et al.*, TED, 2022. [11] S. Wahid *et al.*, IEDM, 2022. [12] Y. Kang *et al.*, VLSI, 2023. [13] D. Zheng et al., IEDM, 2022. [14] Y. Liang *et al.*, VLSI, 2023. [15] S. Samanta *et al.*, VLSI, 2020. [16] J. Liu et al., IEDM, 2021. [17] J. Zhang *et al.*, VLSI, 2023. [18] J. Chiu *et al.*, VLSI, 2023. [19] K. Huang *et al.*, VLSI, 2022. [20] Q. Kong *et al.*, IEDM, 2022. [21] Z. Zhang *et al.*, VLSI, 2023. [22] K. Hikake *et al.*, VLSI, 2023. [23] J. Zhang *et al.*, EDL, 2023. [24] J. Zhang *et al.*, APL, 2022. [25] H. Kawai *et al.*, IEDM, 2020. [26] A. Charnas *et al.*, TED, 2022.

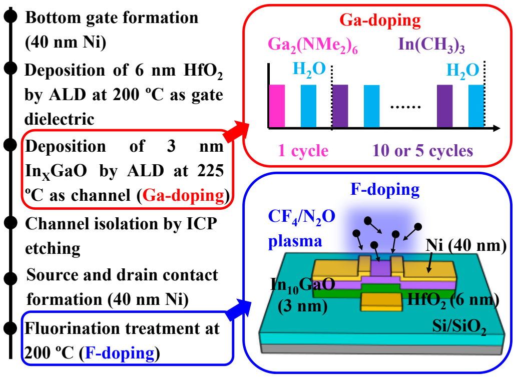

Fig. 1. Process flow of ultrathin InGaO TFTs with T_{ch} of 3 nm, where the Ga- and F-doping are respectively achieved by ALD cycles and CF_4/N_2O plasma.

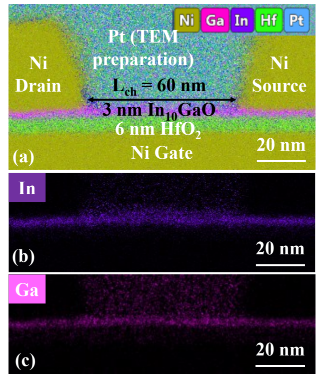

Fig. 2. (a) STEM image of InGaO TFTs with L_{ch} 60 nm, and EDX mapping of (b)In; (c) Ga element.

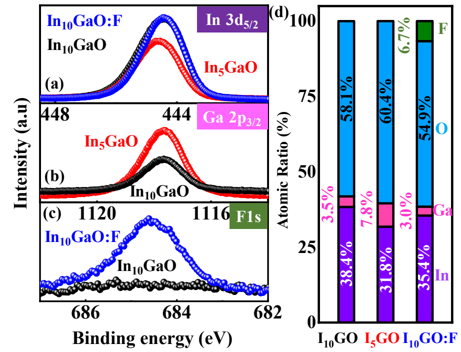

Fig. 3. XPS spectrum of (a) In $3d_{5/2}$; (b) Ga $2p_{3/2}$; (c) F 1s, and (d) derived elemental ratio for InGaO films of different Ga-doping level ($In_{10}GaO$/In_5GaO) or F-doping ($In_{10}GaO:F$).

- ✓ First demonstration of fluorine-doped InGaO TFTs with L_{ch} down to 60 nm and T_{ch} down to 3 nm
- ✓ Novel fluorination method at 200 °C with BEOL compatibility
- ✓ E-mode operation with highest I_{on}/I_{off} of ~10^{11} (I_{off}@V_G of 0 V), high I_{on} of 418 μA/μm and low SS of 85 mV/dec
- ✓ Significantly alleviated self-heating effect with better current saturation
- ✓ Excellent temperature stability with V_T shift of 3.1 mV/ °C
- ✓ Comprehensive gate bias stability study with remarkably high PBTS stability at 80 °C
- ✓ Strategy of overcoming mobility-stability trade-off by fluorination

Fig. 4. Main achievements and highlights of this work.

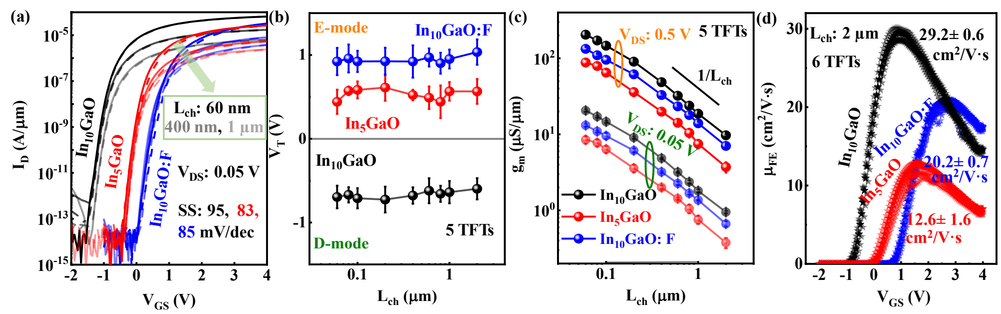

Fig. 5. (a)Transfer curves of $In_{10}GaO$, In_5GaO, $In_{10}GaO:F$ TFTs with L_{ch} of 1 μm, 400 nm and 60 nm. (b) Extracted V_T as a function of L_{ch} from linear extrapolation, suggesting that both Ga- and F-doping could achieve E-mode operation. (c) Extracted g_m as a function of L_{ch}, following $1/L_{ch}$ trend. (d) Extracted μ_{FE} from TFTs with L_{ch} of 2 μm, suggesting that F-doping could achieve higher μ_{FE} than that of Ga-doping.

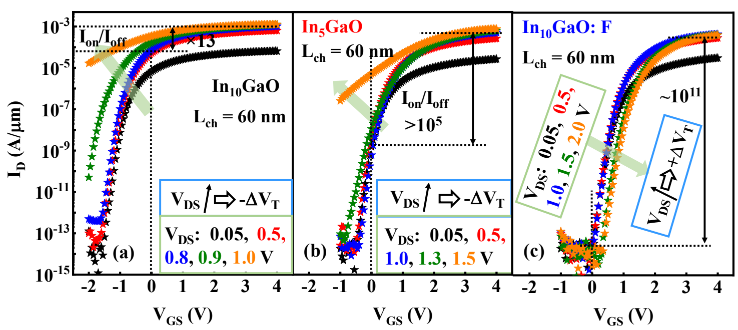

Fig. 6. Transfer curves of (a) $In_{10}GaO$; (b)In_5GaO; and (c) $In_{10}GaO:F$ TFTs with L_{ch} of 60 nm under various V_{DS}. Both $In_{10}GaO$ and In_5GaO TFTs show significantly negative V_T shift under high V_{DS}, in contrast to that $In_{10}GaO:F$ could sustain high V_{DS} with a higher I_{on}/I_{off} of 10^{11} (I_{off}@ V_{GS} of 0 V).

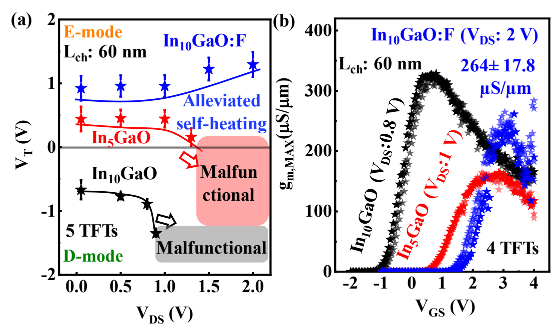

Fig. 7. (a) Extracted V_T (L_{ch}:60 nm) as a function of V_{DS}, where F-doped TFTs show wider operation range due to alleviated self-heating; (b) Extracted $g_{m,MAX}$ for TFTs under various V_{DS}. F-doped TFTs show a high g_m of 264 μS/μm.

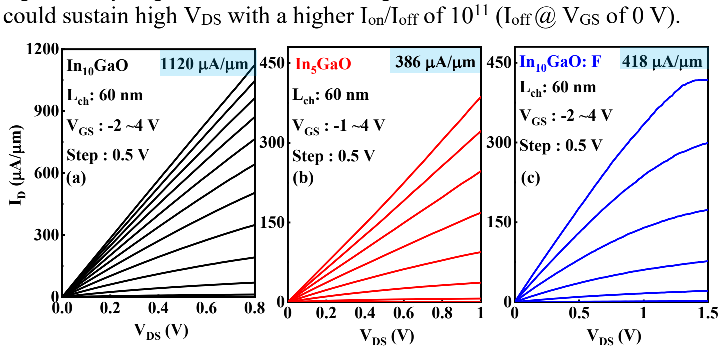

Fig. 8. Output characteristics of (a) $In_{10}GaO$; (b)In_5GaO; and (c) $In_{10}GaO:F$ TFTs with L_{ch} of 60 nm, showing respective I_{on} of 1120, 386 and 418 μA/μm. F-doped TFTs exhibit better saturation due to larger achievable V_{DS}.

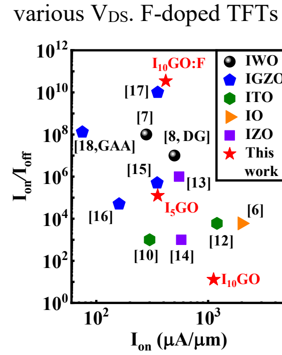

Ref	T_{ch} (nm)	L_{ch} (nm)	V_{DS} (V)	V_{GS} (V)
[6]	1.5	40	0.7	3
[7]	7	100	1.4	2.5
[8]	5	50	0.7	2
[10]	2.1	60	0.8	2
[12]	2	50	1	3
[13]	3.5	100	2.5	2.5
[14]	2	8	1	2
[15]	3.6	38	2.5	3
[16]	8	45	3.6	3.6
[17]	1.5	60	1.2	4
[18]	6	52	3	5
This work	3	60	0.8/1/1.5	4

TFTs are back gate structure unless otherwise noted.

Fig. 9. Benchmark of I_{on}/I_{off} versus achievable I_{on} of oxide TFTs. TFT dimension and bias condition are listed in Table. We show firstly the scaled IGO TFTs with highest I_{on}/I_{off}.

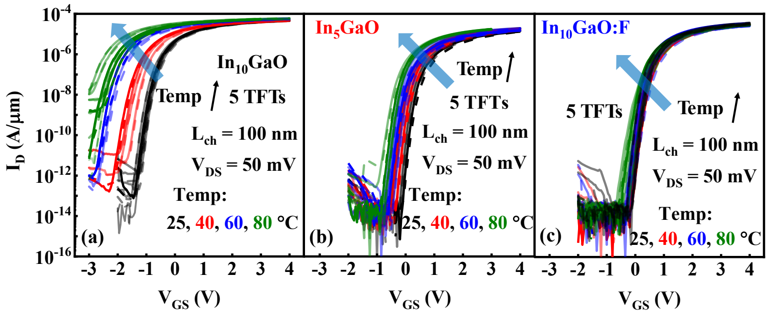

Fig. 10. Transfer curves of (a) $In_{10}GaO$; (b)In_5GaO; and (c) $In_{10}GaO$:F TFTs with L_{ch} of 100 nm under temperature from 25 to 80 °C, where 5 TFTs were measured.

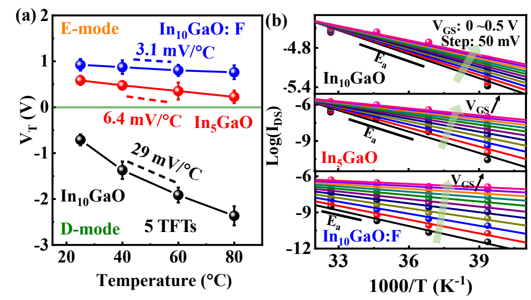

Fig. 11. (a) Extracted V_T as function of temperature. (b) Temperature dependence of I_{DS} for E_a extraction.

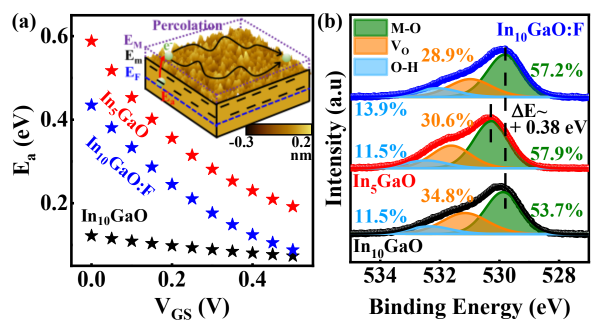

Fig. 12. (a) Activation energy (E_a) as function of V_{GS}. Inset: AFM scan with illustration of percolation mechanism. (b) O 1s spectrum suggests the reduced V_o by Ga- or F-doping.

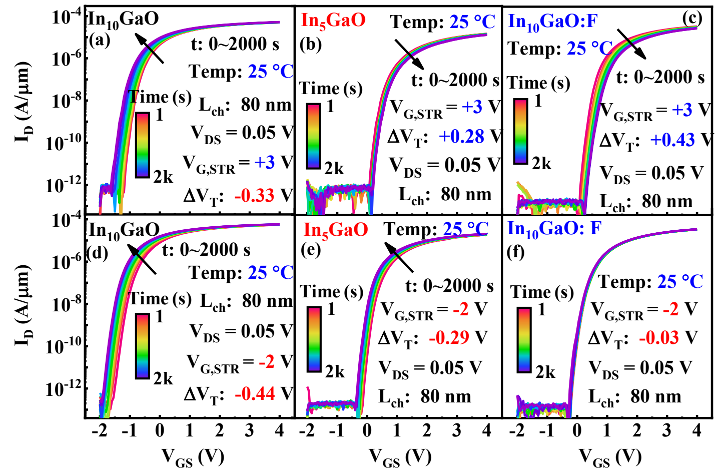

Fig. 13. Transfer curve evolution of $In_{10}GaO$/In_5GaO/$In_{10}GaO$:F TFTs (L_{ch}:80 nm) under (a-c) PBS of +3 V; and (d-f) NBS of -2 V at 25 °C.

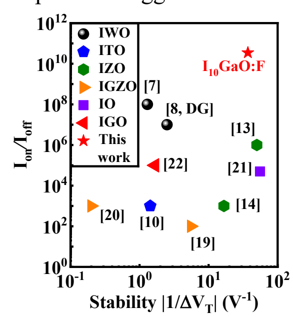

Ref	T_{ch} (nm)	L_{ch} (nm)	E_{OX} (MV/cm)	Temp (°C)
[7]	7	100	3	25
[8]	5	50	3	25
[10]	2.1	60	6	25
[13]	3.5	100	6	25
[14]	2	8	5	25
[19]	3	55	2.5	80
[20]	1.5	40	4	100
[21]	1.6	1000	4	25
[22]	5	10000	1.5	25
This work	3	100	3.4	80

Fig. 17. Benchmark of I_{on}/I_{off} versus stability $|1/\Delta V_T|$ of oxide TFTs. TFT dimension and stress condition are listed in right Table. ΔV_T is compared at 1 ks stress time.

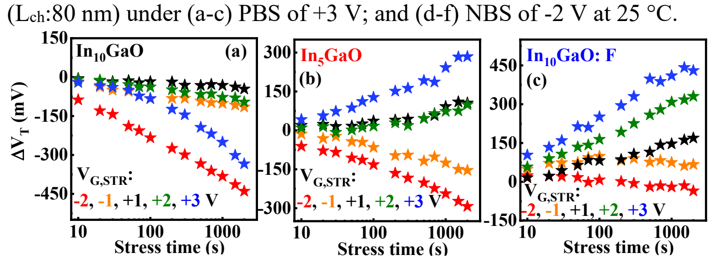

Fig. 14. Time evolution of ΔV_T of (a) $In_{10}GaO$;(b) In_5GaO;(c) $In_{10}GaO$:F TFTs (L_{ch}:80 nm) under $V_{G,STR}$ from -2 V to +3 V at 25 °C up to 2 ks.

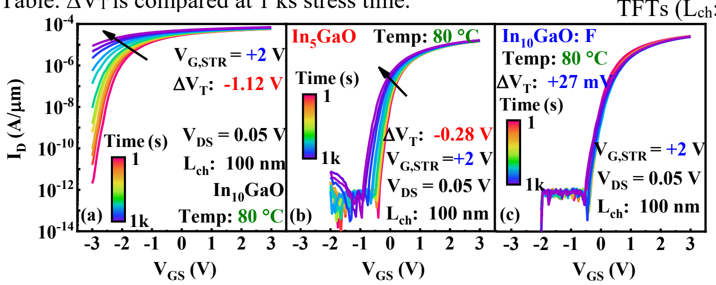

Fig. 15. Transfer curve evolution of (a) $In_{10}GaO$;(b) In_5GaO;(c) $In_{10}GaO$:F TFTs (L_{ch}:100 nm) under PBTS test ($V_{G,STR}$ of +2 V, 80 °C).

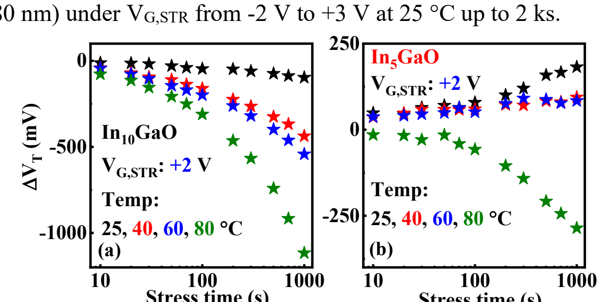

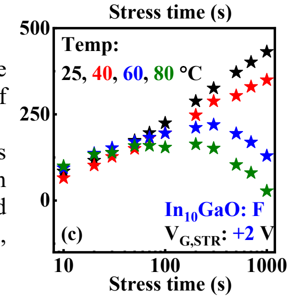

Fig. 16. Time evolution of ΔV_T of (a)$In_{10}GaO$;(b)In_5GaO;(c)$In_{10}GaO$:F TFTs under PBTS test with $V_{G,STR}$ of +2 V and temperature of 25, 40, 60, 80 °C up to 1 ks.

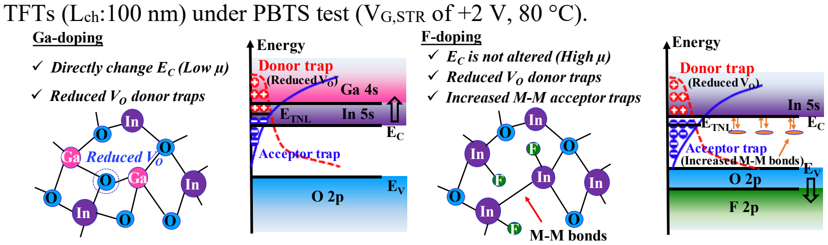

Fig. 18. Comparison of Ga- and F-doping, where F-doping could deliver better mobility-stability trade-off.